Teng Zhou[1]
Jian Ge[1]
Liuyong Shi[1]
Junqing Fan[1]
Zhenyu Liu[2]
Sang Woo Joo[3]

[1]Mechanical and Electrical Engineering College, Hainan University, Haikou, Hainan, P. R. China
[2]Changchun Institute of Optics, Fine Mechanics and Physics (CIOMP), Chinese Academy of Science, Changchun, Jilin, P. R. China
[3]School of Mechanical Engineering, Yeungnam University, Gyongsan, Korea

Received June 19, 2017
Revised November 13, 2017
Accepted November 13, 2017

Research Article

Dielectrophoretic choking phenomenon of a deformable particle in a converging-diverging microchannel

The translational motion of small particles in an electrokinetic fluid flow through a constriction can be enhanced by an increase of the applied electric potential. Beyond a critical potential, however, the negative dielectrophoresis (DEP) can overpower other forces to prevent particles that are even smaller than the constriction from passing through the constriction. This DEP choking phenomenon was studied previously for rigid particles. Here, the DEP choking phenomenon is revisited for deformable particles, which are ubiquitous in many biomedical applications. Particle deformability is measured by the particle shear modulus, and the choking conditions are reported through a parametric study that includes the channel geometry, external electric potential, and particle zeta potential. The study was carried out using a numerical model based on an arbitrary Lagrangian-Eulerican (ALE) finite-element method.

Keywords:
DEP choking / Dielectrophoresis (DEP) / Electrokinetic flow / Microfluidics
DOI 10.1002/elps.201700250

1 Introduction

Precise control of the motion of small particles is one of the most essential pursuits of microfluidics, which has vast applications in chemical research and biomedical studies [1, 2]. Many advances have been made in topics associated with this goal, including dielectrophoresis [3, 4], hydrophoresis [5], magnetophoresis [6–8], and inertial methods [9–11]. Dielectrophoresis has drawn particular attention due to its preciseness and appropriateness for biological particles [12–15]. It results in translational motions of particles due to either induced electrical dipoles (in viruses, particles, polymer beads, cells, etc.) or native electrical dipoles (in proteins, etc.) in an electric-field gradient.

Particles in microfluidic devices go through many geometrical changes, including curved channels and constrictions, and experience a variety of DEP forces. In fluids flowing through a constriction or a converging-diverging channel particles experience a negative DEP force due to a direct-current (DC) electrokinetic flow, which retards the translational motion of particles going into the constriction. With increases in the electric potential applied to the electroosmotic flow, the phoretic motion of the particles would be enhanced, but the DEP retardation is increased as well. Due to its quadratic growth with the increase in electric potential, the DEP retardation can surpass other effects to block particles near the entrance of the constriction. Particles even smaller than the throat of the constriction are thus prevented from passing through it.

This DEP choking phenomenon has been observed both numerically [12, 13] and experimentally [16, 17]. The phenomenon can be used for particle trapping, concentration, and sorting. Previous numerical work has reported conditions for the DEP choking phenomenon for rigid particles. However, there is still limited understanding of the DEP choking phenomenon for deformable particles in a converging-diverging microchannel. In many biomedical applications, particles can be compliant, and the DEP choking criterion for rigid particles is not applicable. Particles that are expected to be blocked from passing the constriction may still pass through it, resulting in failure in a microfluidic operation. Additional parametric studies on the DEP choking phenomenon are required for deformable particles.

In this study, an arbitrary Lagrangian–Eulerian (ALE) finite-element method was employed to simultaneously account for the particle-fluid-electric field interactions [18–20] that are associated with the DEP choking phenomenon for particles with an elastic modulus. A parametric study was performed to investigate the DEP choking phenomenon of the deformable particles for the first time in a converging-diverging microchannel. Based on the ALE method, the parametric region for the DEP choking phenomenon was

Correspondence: Professor Sang Woo Joo, School of Mechanical Engineering, Yeungnam University, Gyongsan 712–719, Korea
E-mail: swjoo@yu.ac.kr

Abbreviations: ALE, arbitrary Lagrangian-Eulerican; **EDL**, electric double layer

Color Online: See the article online to view Figs. 1, 3-5, 8 and 9 in color.

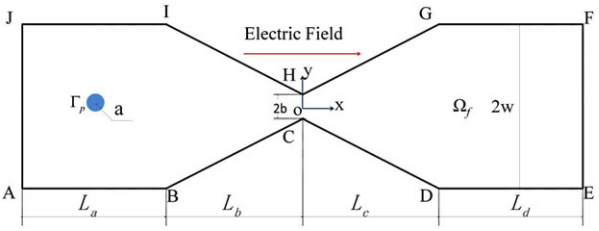

Figure 1. A 2D schematic of the circular particle DEP movement in a converging-diverging microchannel. The origin of the Cartesian coordinate system (x, y) is located at the center of the channel throat with the smallest cross section.

obtained for particles with different shear moduli, among other parameters.

2 Materials and methods

2.1 Mathematical model

Two-dimensional simulations can consistently and efficiently capture the essential physics of electrokinetic flows in microchannels [21–23]. Thus, this study considers a two-dimensional (2D) micro-channel with a uniform inlet section, a converging-diverging constriction, and a uniform outlet section, as shown in Fig. 1. The contraction part of the converging-diverging channel is generated by two symmetrical triangles. An electric potential is applied externally from inlet AJ to grounded outlets EF and to the incompressible Newtonian fluid in domain Ω_f. An electric field $\mathbf{E}$ is generated in the domain by the external potential and induces the electrokinetic motion of a hyper-elastic particle Ω_p suspended in the fluid. The thin-EDL approximation is applied because the electric double layer (EDL) thicknesses adjacent to the charged particle and the channel wall are very thin in comparison to the particle radius and the channel widths [24].

The electrical potential ϕ in the domain Ω_f can be described by the Laplace equation:

$$\nabla^2\phi = 0 \quad \text{in } \Omega_f \tag{1}$$

The local electric field $\mathbf{E}$ can be calculated from the electric potential ϕ:

$$\mathbf{E} = -\nabla\phi \quad \text{in } \Omega_f \tag{2}$$

Since a potential bias is applied across the microfluidic chip, the boundary conditions for ϕ on the right and left boundaries of the microchannel are:

$$\phi = \phi_0 \quad \text{on AJ} \tag{3}$$

and

$$\phi = 0 \quad \text{on EF} \tag{4}$$

The solid boundaries include the channel wall (Γ_w) and particle surface (Γ_p) and are electrically insulating, which yields:

$$\mathbf{n}\cdot\nabla\phi = 0 \text{ on } \Gamma_w \text{ and } \Gamma_p, \tag{5}$$

where $\mathbf{n}$ is a unit outward normal vector.

The Reynolds number in the microchannel is very small, and the conservation of momentum and mass can be described by the Stokes and the continuity equations [25,26]:

$$\rho_f\frac{\partial\mathbf{u}}{\partial t} = \nabla\cdot[-p\mathrm{I} + \mu(\nabla\mathbf{u} + \nabla\mathbf{u}^{\mathrm{T}})] \quad \text{in } \Omega_f \tag{6}$$

and

$$\nabla\cdot\mathbf{u}=0 \quad \text{in } \Omega_f \tag{7}$$

where ρ_f and μ are the density and the viscosity of fluid, respectively, $\mathbf{u}$ and p are the velocity vector and the hydrodynamic pressure, $\mathbf{I}$ is the unit tensor, and $\nabla\mathbf{u}^{\mathrm{T}}$ is the transpose of the velocity gradient $\nabla\mathbf{u}$. An open boundary condition is specified at the inlet AJ and the outlets EF:

$$\nabla\cdot[-p\mathrm{I} + \mu(\nabla\mathbf{u} + \nabla\mathbf{u}^{\mathrm{T}})] = 0 \quad \text{on AJ and EF} \tag{8}$$

The Smoluchowski slip boundary condition for Newtonian electroosmotic flow (EOF) is applied on the charged channel wall:

$$\mathbf{u} = \mathbf{u}_w = \frac{\varepsilon_f\zeta_w}{\mu}(\mathbf{I} - \mathbf{nn})\cdot\nabla\phi \quad \text{on } \Gamma_w\ , \tag{9}$$

where $\mathbf{u}_w$ is the fluid velocity on the channel wall, and ε_f and ζ_w are the fluid permittivity and the zeta potential of the channel wall, respectively. The velocity $\mathbf{u}_p$on the particle consists of two parts: (i) the Smoluchowski slip velocity arising from the particle surface charge and (ii) the velocity of the particle motion. The boundary condition on the particle surface is then:

$$\mathbf{u} = \mathbf{u}_p = \frac{\varepsilon_f\zeta_p}{\mu}(\mathbf{I} - \mathbf{nn})\cdot\nabla\phi + \frac{\partial\mathbf{S}}{\partial t} \quad \text{on } \Gamma_p\ , \tag{10}$$

where ζ_p is the zeta potential of the particle, and $\mathbf{S}$ is the displacement of the deformable particle caused by the particle deformation and movement, which is governed by:

$$\rho_p\frac{\partial^2\mathbf{S}}{\partial t^2} - \nabla\cdot\boldsymbol{\sigma}(\mathbf{S}) = 0 \quad \text{in } \Omega_p \tag{11}$$

Here, ρ_p is the density of the deformable particle, and $\boldsymbol{\sigma}(\mathbf{S})$ is the Cauchy stress in the solid phase, which is considered as a function of the displacement of the particle.

The force on the particle–fluid interface consists of hydrodynamic and electrokinetic stresses:

$$\sigma_p\cdot\mathbf{n}_p = \sigma_f\cdot\mathbf{n}_f + \sigma_E\cdot\mathbf{n}_f \tag{12}$$

$$\sigma_f = -p\mathrm{I} + \mu(\nabla\mathbf{u} + \nabla\mathbf{u}^{\mathrm{T}}) \tag{13}$$

$$\sigma_E = \varepsilon_f\mathbf{EE} - \frac{1}{2}\varepsilon_f(\mathbf{E}\cdot\mathbf{E})\mathbf{I} \tag{14}$$

where σ_p, σ_f, and σ_E are the total stress tensor on the particle surface, the hydrodynamic stress tensor, and the Maxwell stress tensor, respectively.

In the simulations, the particle is considered as an incompressible Neo–Hookean material expressed as:

$$W_s = \frac{1}{2}G_0(I_C - 3) \tag{15}$$

$$\sigma(\mathbf{S}) = J^{-1}\mathrm{P}\mathrm{F}^{\mathrm{T}} \tag{16}$$

$$\mathrm{P} = \frac{\partial W_s}{\partial \nabla_X \mathbf{S}} \tag{17}$$

$$\mathbf{C} = \mathbf{F}^{\mathrm{T}}\mathbf{F} \tag{18}$$

$$\mathbf{F} = \nabla\mathbf{S} + \mathrm{I} \tag{19}$$

Here, W_s is the energy density function, G_0 is the shear modulus of the hyperelastic particle, $I_C = \mathrm{tr}(\mathbf{C})$ is the first invariant of the right Cauchy–Green tensor, $\mathbf{F}$ is the deformation gradient tensor, J is the determinant of the deformation gradient tensor $\mathbf{F}$, $J = 1$ for the incompressible Neo–Hookean material, and $\mathbf{P}$ is the first Piola–Kirchhoff stress.

The half width of the throat b, the zeta potential of the channel wall ζ_w, and the electrophoretic velocity $U_\infty = (\varepsilon_f \xi_w/\mu)(\xi_w/b)$ are used as the characteristic length, characteristic electric potential, and characteristic velocity to normalize the governing equations, respectively. Based on the system of governing Eqs. (1)- (19), the electric field E and the time t are scaled by $b/((\varepsilon_f \xi_w/\eta)(\xi_w/b))$ and ζ_w/b. Thus, the governing system is nondimensionalized to:

$$\mathrm{Re}\frac{\partial \mathbf{u}^*}{\partial t^*} = -\nabla^* \cdot [-p^*\mathrm{I} + (\nabla^*\mathbf{u}^* + \nabla^*\mathbf{u}^{*\mathrm{T}})] \quad \text{in } \Omega_f \tag{20}$$

$$\nabla^*\mathbf{u}^* = 0 \quad \text{in } \Omega_f \tag{21}$$

$$\nabla^{*2}\phi^* = 0 \quad \text{in } \Omega_f, \tag{22}$$

$$\mathrm{Re}\frac{\rho_p}{\rho_f}\frac{\partial^2 \mathbf{S}^*}{\partial t^{*2}} - \nabla^* \cdot \sigma(\mathbf{S}^*) = 0 \quad \text{in } \Omega_p \tag{23}$$

where $\mathbf{u}^*$, p^* and ϕ^* are the dimensionless velocity, pressure, and electrical potential, respectively.

2.2 Numerical method and code validation

The density ρ_f and the dynamic viscosity μ of the Newtonian fluid are set to 1000 kg/m^3 and 0.001 Pa · s. The particle density ρ_p is set to be the same as the density of the fluid ρ_f. The permittivity ε_f is chosen as 7.08×10^{-10} F/m, and the uniform zeta potential of the wallζ_w is equal to −80 mV. The converging-diverging section of the channel is symmetric, and $L_b = L_c = 400\ \mu m$ with respect to the throat where the cross section is minimal, while the width of the throat is $b = 27.5\ \mu m$. The particle moves from left to right.

The governing systems of equations are solved using the commercial finite element package COMSOL (version 4.3a, www.comsol.com) coupled with MATLAB in a high-performance cluster. The coupled system of the hydrodynamics, electrical field, and particle dynamics is solved simultaneously. The finite-element mesh deforms while following the motion of the particle in the ALE method, and its quality is reduced as the particle moves in the microfluidic channel. There are more than 20 000 total elements with a minimum of 100 elements positioned adjacent to the particle surface based on rigorous mesh-refinement tests. The mesh element quality is a dimensionless quantity between 0 and 1, where 1 represents a perfectly regular element in the chosen quality measure, and 0 represents a degenerated element. The COMSOL computations include the default mesh quality measures method [27], which was used in this simulation. Before the mesh quality decreases below 0.7 out of a maximum 1.0 when the particle moves, the domain of the system is re-meshed with the current position of the particle. The computational process is restarted after the solution is mapped to the new mesh.

We also compared the numerical predictions with the results from Ai and Qian [13] for the electrophoresis of a spherical particle in a converging-diverging channel with a dimensionless electric field intensity $E^* = 17.19$. This intensity is calculated by dividing the dimensionless electric potential difference between the inlet and outlet over the dimensionless length of the entire microchannel. The zeta potential ratios $\gamma = 0.4$ ($\gamma = \zeta_p/\zeta_w$). To simulate a rigid particle, we used an extremely large value for the shear modulus, $G = 2000$ Pa. As shown in Fig. 2, the numerical predictions with the present method (solid line) are in good agreement with those of Ai and Qian (symbols).

3 Results and discussion

In this section, the particle movement with different shear moduli is presented to show the DEP choking phenomenon for deformable particles. A parametric study was performed to investigate the effects of the shear modulus in relation to the critical dimensionless width w^* and the dimensionless electric field intensity E^*. The electric field and zeta potential

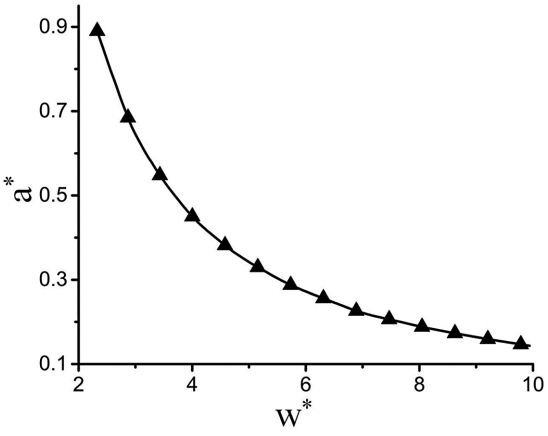

Figure 2. Critical non-dimensional particle radius a^* for the DEP choking regions as a function of the non-dimensional width w^* of the converging-diverging channel. Choking occurs in the region above each bounding curve. The particle with a shear modulus of G = 2000 Pa can be regarded as a rigid particle ($E^* = 17.19$, $\gamma = 0.4$). The triangle symbol and solid line represent the numerical solution from Ai and Qian [13] and the numerical results from the present model, respectively.

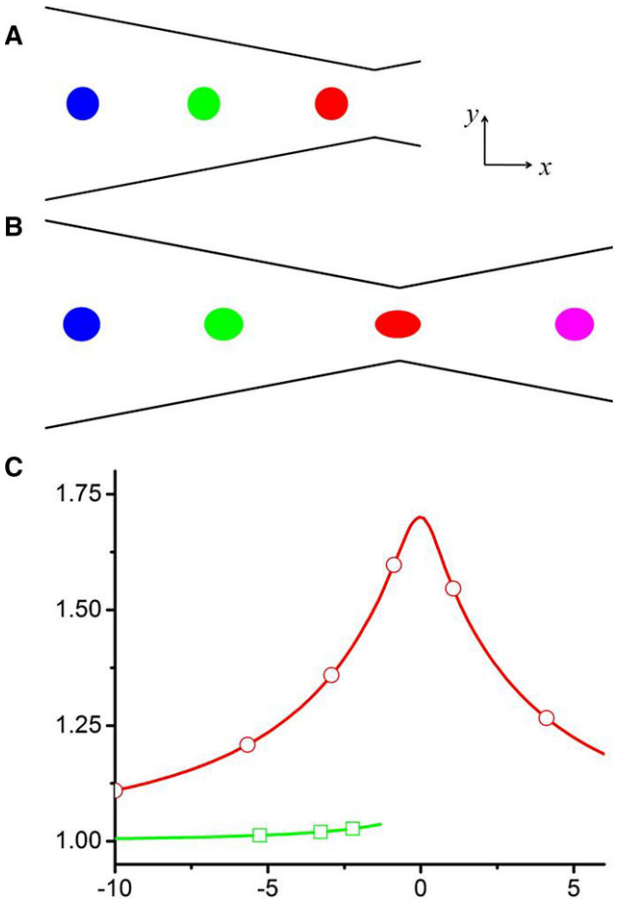

Figure 3. Particles with (A) G = 200 Pa and (B) G = 10 Pa moving in the converging-diverging channel. $E^* = 17.19$, $\gamma = 0.4$, $w^* = 3.68$, $a^* = 0.5$. The non-dimensional x coordinates of the particle position in blue, green, red, and magenta are -9, -5, 0, and 5. (C) The ratio of the major (x-direction) to minor (y-direction) axis of the particle for G = 10 (circle) and 200 (square) Pa. $E^* = 17.19$, $\gamma = 0.4$, $w^* = 3.68$, $a^* = 0.5$.

ratio versus the particle size were also studied to show the feasibility of particle manipulation based on the DEP choking phenomena for different zeta potential ratios and particle sizes.

3.1 The DEP choking phenomenon

Figure 3 shows the particle shape at different stream-wise positions along the microchannel for shear moduli of G = 10 and 200 Pa. The applied dimensionless electric field intensity is $E^* = 17.19$, the potential ratio is $\gamma = 0.4$, the dimensionless width is $w^* = 3.68$, the dimensionless particle radius is $a^* = 0.5$, which correspond to a point in the DEP choking region for a rigid particle in Fig. 2. The non-dimensional x-coordinates of the particle position in blue, green, red, and magenta indicate −9, −5, 0, and 5. The simulation results show that the deformable particle with a shear modulus of $G = 10$ Pa passes through the throat, while a more rigid particle with a shear modulus of $G = 200$ Pa is blocked at the constriction entrance. A more compliant particle with a low shear modulus deforms itself into an elliptical shape to overcome the adverse DEP effect to pass the constriction. As it moves toward the throat, it is squeezed gradually in the $y$direction, passes through the entire constriction, and recovers its circular shape. However, a more rigid particle with $G = 200$ Pa is much less compliant and does not deform enough to pass the constriction.

Figure 3C shows the degree of particle deformation by the ratio of the major axis to the minor axis of the particle for two different values of G. For the more compliant particle ($G = 10$ Pa), deformation or flattening increases as the particle approaches the constriction before its shape is gradually recovered. For the less compliant particle ($G = 200$ Pa), the deformation is less conspicuous, and it stops before the particle enters the throat of the channel due to the choking phenomenon. Thus, the results shown in Fig. 3 reveal that high deformability allows the particle with low shear modulus to pass through the throat, while the more rigid particle without sufficient deformation experiences DEP choking.

The DEP force along the center line of the channel will retard the particle moving into the channel center by affecting the total force, so it is reasonable to study the total force on the particle. Due to the different shapes, there is different net force in the same location, including the DEP and the hydrodynamic force on the particles that push the particle downstream in the channel. The x-component of the non-dimensional total force is computed for each of the two different shapes to demonstrate that the net force on the particles depends on the shape of particle. The position of particles in the $y$direction is set to the center of the channel. Figure 4 illustrates the non-dimensional force, which shows a gradual decrease as the particle approaches the constriction. The non-dimensional force for the circular particle decreases

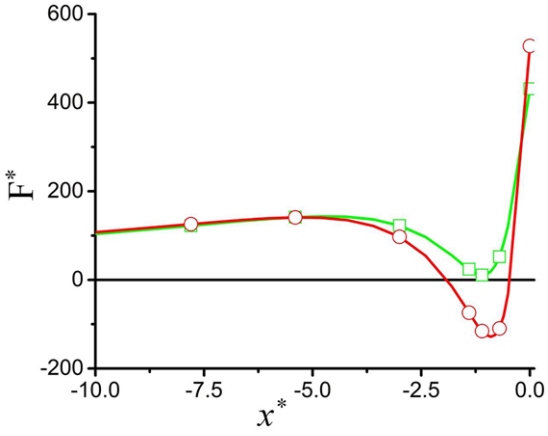

Figure 4. Non-dimensional total force F^* applied on circular and elliptical particles with same the same area in the converging-diverging channel. $E^* = 20$, $w^* = 4$, gamma = 0.4, a^* of the circular particle is 0.5, and the ratio of the non-dimensional long axis to the short axis of the elliptical particle is 2. The red line with the circular symbols and the green line with the square symbols represent the circular and elliptical particles, respectively.

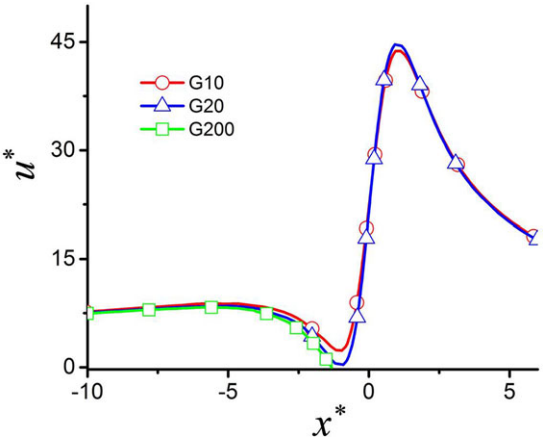

Figure 5. Non-dimensional velocity component u^* in the x direction of particles with shear moduli of G = 10, 20, 200 Pa when they are moving from the left to the right in the converging-diverging channel. $E^* = 17.19$, $\gamma = 0.4$, $w^* = 3.68$, $a^* = 0.5$. The red line with the circular symbols, the blue line with triangular symbols, and the green line with the square symbols represent particles with shear moduli of G = 10, 20, and 200 Pa, respectively.

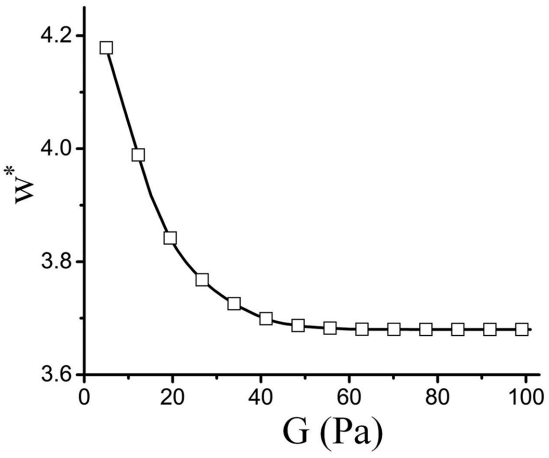

Figure 6. Critical non-dimensional width w^* of the converging-diverging channel for the DEP choking regions as a function of the shear modulus G of the particle. The choking occurs in the region above each bounding curve. $E^* = 17.19$, $\gamma = 0.4$, $a^* = 0.5$.

to negative values before the constriction throat. Thus, it is expected that the circular particle will not advance into the throat. Using this mechanism, particles with different shear modules can be separated.

The particle's translational velocity magnitude indicates whether the DEP choking phenomenon exists. The difference in the streamwise translation velocity of a particle is induced by the difference of the net force on the particles due to the shear modulus. The streamwise translation velocity difference of particles is shown in Fig. 5 in the *x*direction for the more rigid particle with $G = 200$ Pa gradually decreases to zero before the center of the throat, resulting in DEP choking. The translational velocities for the deformable particles with $G = 10$ Pa and $G = 20$ Pa decrease initially but increase back as the particles take on a squeezed elliptical shape.

Before the center of the throat, the DEP force on the particle retards its motion into the converging part of the channel. After the narrowest part of the throat, the DEP force promotes its motion out of the diverging part of the channel. The particles are thus accelerated in the diverging section with higher velocity than they have in the symmetric converging section. The deformed particles recover their circular shape as they pass through the throat, after which the particle velocity exhibits little dependence on the shear modulus, as shown in the magenta color position of Fig. 3B for $G = 10$ Pa and $G = 20$ Pa.

3.2 Channel width versus shear modulus

No matter how large the particle size and the electric field intensity are, it is impossible for straight uniform microchannels to induce the DEP choking phenomenon. The nonuniformity of the electric field caused by the constriction ratio is the essential reason for the DEP choking phenomenon. Figure 6 illustrates the critical non-dimensional width w^* of the converging-diverging channel for the DEP choking region as a function of the shear modulus G of the particle. The choking occurs in the region above each bounding curve. Here, the applied dimensionless electric field intensity is $E^* = 17.19$, the potential ratio is $\gamma = 0.4$, and the dimensionless particle radius is $a^* = 0.5$.

The results indicate that a particle with low shear modulus requires a higher constriction ratio in order to generate a higher nonuniformity of the electric field for the DEP choking. The result also shows that the DEP choking force on a particle with low shear modulus is less than that of a particle with high shear modulus under the same constriction ratio. Therefore, sequential converging-diverging channels with different constriction ratios can be designed to selectively trap cells with different shear modulus, which is an important marker of the condition of biological particles such as cells. They can then be separated from complex mixtures based on their different shear modulus. This is a prerequisite step for many biological analyses. Using the same principle, a suitable constriction ratio can be used to separate cells with a chosen shear modulus when the dimensionless electric field intensity and other parameters are chosen for particular applications.

3.3 Electric field versus shear modulus

The magnitude of the applied electric field intensity influences the nonuniformity of the electric field. When other parameters are the same, the nonuniformity of the electric field increases with the magnitude of the electric field intensity. Figure 7 shows the DEP choking regions of deformable particles according to the external electric field, and the choking region is above the line. Here, a potential ratio of $\gamma = 0.4$ is employed for the dimensionless particle radius $a^* = 0.5$

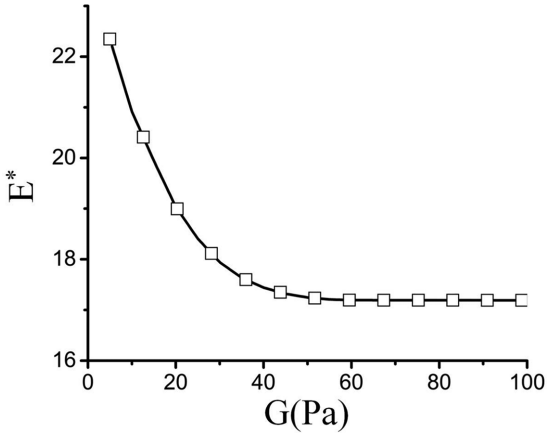

Figure 7. Critical non-dimensional electric field E^* of the converging-diverging channel for the DEP choking regions as a function of the shear modulus G of the particle. The choking occurs in the region above each bounding curve. $w^* = 3.68$, $\gamma = 0.4$, $a^* = 0.5$.

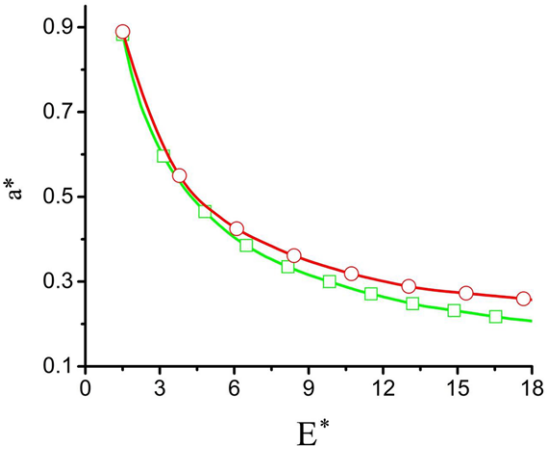

Figure 8. Critical non-dimensional particle radius a^* for the DEP choking regions as a function of the non-dimensional electric field intensity E^*. The choking occurs in the region above each bounding curve. $\gamma = 0.6$, $w^* = 5.9$. The red line with the circular symbols and the green line with the square symbols represent particles with shear moduli of G = 10 and 200 Pa, respectively.

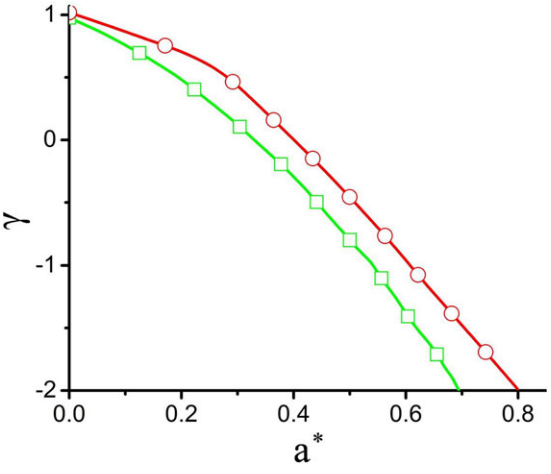

Figure 9. Critical zeta potential ratio γ for the DEP choking regions as a function of the non-dimensional particle radius a*. The choking occurs in the region above each bounding curve. $E^* = 17.19$, $w^* = 5.9$. The red line with the circular symbols and the green line with the square symbols represent particles with shear moduli of G = 10 and 200 Pa, respectively.

and the non-dimensional width $w^* = 3.68$. It is consistently shown that the choking region expands as the particle shear modulus increases. The particles with low shear modulus require higher electric field intensity for the DEP choking. It is demonstrated that particle sorting according to the shear modulus can be achieved by adjusting the applied voltage between the inlet and the outlet of a microchannel with a fixed geometry.

Figure 7 shows that the absolute value of the function between the external electric field and the particle shear modulus decreases when the shear modulus of the particle increases. When the particle shear modulus is low, the absolute value of the value is very large. The value then gradually decreases to zero after the shear modulus increases to a certain level. The phenomenon shows that the sensitivity of the deformability of the flexible particle to the electrical field increases when the particle shear modulus decreases. In the other words, there is less difference in the electrical intensity for distinguishing a particle with a different shear modulus when the shear modulus is low. Thus, the choking phenomenon can easily be used for sorting particles with a lower modulus by the converging-diverging channel.

3.4 Electric field versus particle size

Smaller particles require larger electric field intensity for DEP choking. Similarly, low-modulus particles require larger electric field intensity for DEP choking. Figure 8 shows the regions for DEP choking of particles with G = 10 Pa and 200 Pa in an electric field E^* versus the particle size a^* for a zeta potential ratio of $\gamma = 0.4$ and constriction ratio of $w^* = 5.9$. The red line with the circular symbols and the green line with the square symbols represent the particles with shear moduli of G = 10 and 200 Pa, respectively. For both cases, the required electric field E^* for the DEP choking approaches infinity as the particle radius a^* approaches zero. As the particle size increases, E^* decreases. E^* of the particle with G = 10 Pa is higher than that of the particle with G = 200 Pa. The critical electric field increases as the particle modulus decreases, which is consistent with the results in Fig. 7. Hence, particles with identical size but different shear modulus can be separated effectively by adjusting the electric field intensity.

3.5 Particle size versus zeta potential ratio

Figure 9 shows the DEP choking region for the particle size a^* versus the zeta potential ratio γ for particles with G = 10 Pa and 200 Pa, an electric field of $E^* = 17.19$, and a constriction

ratio of $w^* = 5.9$. It is consistently shown that the choking region decreases with the decreasing shear modulus. If the zeta potential ratio is positive, the particle and the channel wall are negatively charged. As a result, the particle electrophoresis retards the particle moving toward the converging-diverging channel. Thus, for both particles, the total driving force that pushes the particle to the center decreases as the zeta potential ratio increases until it vanishes at 1.

When the zeta potential ratio decreases from a positive value to a negative value, the net retarding force on both particle surfaces with G = 10 Pa and G = 200 Pa decreases. As the negative zeta potential accelerates the particle motion, the critical particle size for the DEP choking increases gradually to 1 when the zeta potential ratio γ decreases. However, the net retarding force on the particle surface with G = 10 Pa decreases faster than that of the particle with G = 200 Pa due to the deformation of the particle. Thus, the result once again illustrates that the converging-diverging microchannel can be used for sorting and trapping particles with different shear moduli.

4 Concluding remarks

The DC DEP choking phenomenon of deformable particles through a converging-diverging microchannel was quantitatively studied using a transient ALE finite-element method and thin-EDL approximation. A parametric study was performed to investigate the DEP choking phenomenon, including the channel width versus the shear modulus, the electric field intensity versus the shear modulus, the electric field versus the particle size, and the particle size versus the zeta potential ratio. The particle movement process obtained by the simulation shows that a more compliant particle with low shear modulus deforms into a nearly elliptical shape to overcome the adverse DEP effect and pass the constriction. The parametric study revealed that a deformable particle needs higher nonuniformity of the electric field, higher particle size ratio, and higher zeta potential ratio for the DEP choking of particles through a nonuniform microchannel to occur. Thus, the results suggest a design range of the geometry for particles with different shear moduli for particle choking, which could be used for particle sorting, trapping, and concentration, among other applications.

This work was funded by the National Natural Science Foundation of China (Grant No. 51605124), the Scientific Research Foundation of Hainan University (Grant No.Kyqd1569, hdkyxj201721 and hdkyxj201722), and the National Research Foundation of Korea (Grant No. 2015–002423).

The authors have declared no conflict of interest.

5 References

[1] Xuan, X., Zhu, J., Church, C., *Microfluid. Nanofluid.* 2010, *9*, 1–16.

[2] Sajeesh, P., Sen, A. K., *Microfluid. Nanofluid.* 2013, *17*, 1–52.

[3] Ai, Y., Qian, S., *Electrophoresis* 2011, *32*, 996–1005.

[4] Ai, Y., Qian, S., *J. Colloid Interface Sci.* 2010, *346*, 448–454.

[5] Zhou, T., Liu, Z., Wu, Y., Deng, Y., Liu, Y., Liu, G., *Biomicrofluidics* 2013, *7*, 054104.

[6] Qian, S., Bau, H. H., *Mech. Res. Commun.* 2009, *36*, 10–21.

[7] Pamme, N., Manz, A., *Anal. Chem.* 2004, *76*, 7250–7256.

[8] Liang, L., Xuan, X., *Microfluid. Nanofluid.* 2012, *13*, 637–643.

[9] Li, D.-Y., Li, X.-B., Zhang, H.-N., Li, F.-C., Qian, S., Joo, S. W., *Microfluid. Nanofluid.* 2017, *21*, 10.

[10] Zhang, J., Yan, S., Yuan, D., Alici, G., Nguyen, N.-T., Warkiani, M. E., Li, W., *Lab Chip* 2016, *16*, 10–34.

[11] Martel, J. M., Toner, M., *Annu. Rev. Biomed. Eng.* 2014, *16*, 371–396.

[12] Ai, Y., Qian, S., Liu, S., Joo, S. W., *Biomicrofluidics* 2010, *4*, 13201.

[13] Ai, Y., Mauroy, B., Sharma, A., Qian, S., *Electrophoresis* 2011, *32*, 2282–2291.

[14] Ai, Y., Beskok, A., Gauthier, D. T., Joo, S. W., Qian, S., *Biomicrofluidics* 2009, *3*, 44110.

[15] Zhou, T., Yeh, L.-H., Li, F.-C., Mauroy, B., Joo, S., *Micromachines* 2016, *7*, 170.

[16] Zhu, J., Xuan, X., *Electrophoresis* 2009, *30*, 2668–2675.

[17] Kovarik, M. L., Jacobson, S. C., *Anal. Chem.* 2008, *80*, 657–664.

[18] Hu, H. H., Patankar, N. A., Zhu, M. Y., *J. Comput. Phys.* 2001, *169*, 427–462.

[19] Al Quddus, N., Moussa, W. A., Bhattacharjee, S., *J. Colloid Interface Sci.* 2008, *317*, 620–630.

[20] Zhou, T., Shi, L., Fan, C., Liang, D., Weng, S., Joo, S. W., *Microfluid. Nanofluid.* 2017, *21*, 59.

[21] Ai, Y., Joo, S. W., Jiang, Y., Xuan, X., Qian, S., *Electrophoresis* 2009, *30*, 2499–2506.

[22] Ai, Y., Park, S., Zhu, J., Xuan, X., Beskok, A., Qian, S., *Langmuir* 2010, *26*, 2937–2944.

[23] Davison, S. M., Sharp, K. V., *Microfluid. Nanofluid.* 2008, *4*, 409–418.

[24] Zhou, T., Wang, H., Shi, L., Liu, Z., Joo, S., *Micromachines* 2016, *7*, 218.

[25] Zhou, T., Xu, Y., Liu, Z., Joo, S. W., *J. Fluids Eng.* 2015, *137*, 091102.

[26] Zhou, T., Liu, T., Deng, Y., Chen, L., Qian, S., Liu, Z., *Microfluid. Nanofluid.* 2017, *21*, 11.

[27] Comsol, A., *Comsol Multiphysics User's Guide*, Comsol, Sweden 2010.

